Research article

Journal of RAMAN SPECTROSCOPY

Received: 1 October 2014 Revised: 24 December 2014 Accepted: 5 January 2015 Published online in Wiley Online Library

(wileyonlinelibrary.com) DOI 10.1002/jrs.4656

Autonomous soil analysis by the Mars Micro-beam Raman Spectrometer (MMRS) on-board a rover in the Atacama Desert: a terrestrial test for planetary exploration

Jie Wei,[a]* Alian Wang,[a] James L. Lambert,[b] David Wettergreen,[c] Nathalie Cabrol,[d] Kimberley Warren-Rhodes[d] and Kris Zacny[e]

Laser Raman spectroscopy (LRS) has been proposed for *in situ* characterization of molecular species in planetary surface exploration, and three laser Raman spectrometers are included in the science payloads of two under-development missions to Mars (ESA-ExoMars2018 and NASA-Mars2020). We report the first rover test of a laser Raman spectrometer developed for flight, the Mars Micro-beam Raman Spectrometer (MMRS) in the Atacama Desert (Chile). The MMRS was integrated on the Zoë rover and analyzed subsurface samples brought up by a 1 m drill and delivered by a carousel. The MMRS demonstrated robust performance over 50-km traverse on rugged terrains. From MMRS data, igneous minerals, carbonates, sulfates and carbonaceous materials were unambiguously identified. Quantified distributions of major minerals and carbonaceous materials are extracted from MMRS results, which can be used to imply the regional geological evolution, and potential bioactivities. MMRS in the field performed as well as an LRS laboratory instrument when MMRS was focused satisfactorily. The discovery of stable γ-anhydrite, in large quantity (20% in a sample), in the Atacama soils raises an important question of its stability in the field in a natural environment that is worth further laboratory experimental investigation. Copyright © 2015 John Wiley & Sons, Ltd.

Keywords: Mars Micro-beam Raman Spectrometer; rover; soil; Atacama Desert

Introduction

The Atacama Desert extends in northern Chile between the Coastal Range in the west and the Andes in the east. It is one of the driest and oldest deserts in non-polar regions of the Earth. The moist Pacific air is prevented from entering the desert by the combination effects of the elevation of the Coastal Range, the South Pacific Anticyclone, together with the cold Humboldt current traveling along the coast of South America.[1] The precipitation in the Coastal Range averages about 10 mm/year from fog. The precipitation in the eastern region increases with elevation as the Atacama Desert gradually climbs up to the high Andes.[1,2] The interior core of Atacama Desert (~24–25 S, 69–70 W) receives $<<$ 5-mm mean annual rainfall,[3,4] thus serves as an analog for the hyperarid conditions on Mars. Moreover, potential pedogenic processes on Mars during periods of transient aqueous activity may have developed salty soils with chemistry and mineralogy similar to Atacama soils.[5] A variety of sulfates were identified on Mars, whereas nitrate, sulfate and chloride accumulations have a broad distribution in the Atacama Desert. Typical soils show sulfate and chlorine concentrations, similar to that observed on Mars during the Pathfinder and Mars Exploration Rover missions.[5] Thus from the climatic, mineralogical and geochemical standpoints, the Atacama Desert is a relevant terrestrial analog site to early Mars.[6] It is also a relevant site for testing the robustness of an instrument developed for space flight and its autonomous operation procedures for future missions.[2,5]Laser Raman spectroscopy (LRS) is an extremely powerful tool for *in situ* mineralogy for planetary surface exploration missions. Compared with other molecular spectroscopic techniques (NIR and MIR), the key advantage of LRS is that its spectral peaks are sharper and more distinct, which allows direct and unambiguous molecular phase identification from raw Raman spectra of mixtures, i.e. a rock or a soil patch at planetary surfaces. LRS can not only identify major, minor, trace molecular species, but can also quantify molecular proportions, cation ratios, degree of hydration, oxidation states and structural ordering. Furthermore, LRS has a unique capability to detect carbonaceous materials and to characterize organic markers that have the highest preservation potential in harsh environments over long durations.

* *Correspondence to: Jie Wei, Dept of Earth and Planetary Sciences and McDonnell Center for the Space Sciences, Washington University in St. Louis, 1 Brookings Drive, St. Louis, MO 63130, USA.*
E-mail: jiewei@levee.wustl.edu

a *Department of Earth and Planetary Sciences and McDonnell Center for the Space Sciences, Washington University in St. Louis, 1 Brookings Drive, St. Louis, MO 63130, USA*

b *Jet Propulsion Laboratory, 4800 Oak Grove Drive, CA 91109, USA*

c *The Robotics Institute, Carnegie Mellon University, 5000 Forbes Avenue, Pittsburgh, PA, 15213, USA*

d *The SETI Institute, Carl Sagan Center, NASA Ames Research Center, Moffett Field, CA 94035, USA*

e *HoneyBee Robotics and Spacecraft Mechanisms Corporation, 398 West Washington Blvd, Suite 200, Pasadena, CA 91103, USA*

As a result, it is a useful tool for a mission aimed at *seeking the signs of life*. The development of the Mars Micro-beam Raman Spectrometer (MMRS) has been supported by NASA Planetary Instrument Definition and Development Program, and NASA Mars Instrument Development Program.[7–10] Through the life in the Atacama (LITA) project supported by NASA Astrobiology Technology for Exploring Planets program, MMRS got the opportunity to field-test the instrument in the Atacama Desert.

The 2013 LITA field campaign at the Atacama Desert

The primary science goal of LITA is to understand the subsurface distribution of microbial life and habitats across the desert.[2] It also seeks to advance remote exploration in terrestrial extreme environments and future Mars missions.[2] The autonomous Zoë rover, capable of up to 10 km of daily traverse, was designed to explore the extent and distribution of microbial life and habitats across the desert from the relatively wet coastal region to the core of the desert. Previous investigations have found that the wet sites close to the coast had higher diversity and abundance of life compared to the dry sites.[2,11,12] The 2013 LITA exploration deployed and tested a 1-m drill mounted on the autonomous rover for subsurface soil sampling. The MMRS and a bio-generated UV Fluorescence (BUF) imager were among the science instruments that the Zoë rover carried for subsurface soil analysis. It was the first time that a drill for 1-m depth, a micro-beam laser Raman spectrometer (MMRS) and a UV stimulated fluorescence imager (BUF) were integrated together on a rover, and performed autonomous subsurface sample acquisition and analysis to record the poorly known subsurface environment, along a 50-km traverse on ragged terrain.[13] The field exploration was remotely directed by a science team in U.S. and locally operated by an engineering team in the Atacama Desert. The instruments, technologies and science exploration strategies of LITA project have direct relevance to the Mars exploration missions, e.g. ESA-ExoMars2018 and NASA-Mars2020.

The Zoë Rover and the Atacama traverse

The LITA 2013 field operation consisted of a highly mobile rover, autonomous subsurface soil sample collection and delivery, and sample analysis by the two scientific *in situ* sensors (Fig. 1). The Zoë rover was built by the Robotics Institute in the Carnegie Mellon University. It is solar powered, and has the capability of traveling kilometers per day and to autonomously drill to acquire subsurface samples that are analyzed by onboard instruments. During the 10-days' field operation in June 2013, the Zoë rover travelled a ~50-km traverse, covering diverse geomorphologic areas from unconsolidated alluvial fan to dry playa (Fig. 2). The full payloads (including navigation cameras, the drill and the scientific instruments) were installed on the Zoë rover at the landing site and stayed on the rover during the 10-days' operation [Cabrol *et al.*, manuscript in preparation]. The rover and the instruments hibernated overnight and woke up in the morning, using the power generated by the solar panels. The rover, drill and science instruments all experienced large variations of temperature and humidity variations, which were logged by T-RH sensors on board of the Zoë rover. The day and night temperature fluctuated in a range of 36.2 °C from −5.1 °C to 31.1 °C, reaching daily the highest around 15:00 h in the afternoon and the lowest in the early morning before sunrise. The relative humidity changed in a range of 55.9% from 1.8% to 57.7%. It varied with temperature in most cases with low RH at high temperature; however, the absolute humidity calculated from T and RH shows that it fluctuated from 0.30 g/m^3 to 3.93 g/m^3.

Sampling and sample delivering

Autonomous subsurface sampling was carried out by a 1-m drill mounted on the Zoë rover, built by Honeybee Robotics.[14] The drill was designed to capture soil/rock cuttings from depths to approximately 1 m. The sampling system used a 'bite' approach, whereby a drill repeatedly penetrated in 10-cm intervals, captured the sample on the deep flutes and deposited the sample into one of the 20 sample cups (1-cm^3 volume each) on the carousel.[15] The rover controller commanded the carousal to turn, and to position a particular sample cup under the scientific *in situ* instruments for analysis. The sample cups were filled up either autonomously by the drill, or manually by the field operation team.

The end to end operation included drilling to target depths (10 cm, 30 cm and 80 cm), sample capture, sample transfer to a target cup and positioning of the cup underneath scientific *in situ* instruments: MMRS and BUF. The drill managed to successfully capture large volumes of sample in a dry playa (Locales 8–11) where soils were cohesive and fine grained. However at alluvial fans consisting of coarse and highly porous soils containing many large pebbles, the sampling effectiveness was poor. To achieve higher sampling efficiency in these sites (e.g. locale 2B), the auger-drill has been redesigned to use larger diameter and lower pitch flutes. Additional soil samples were collected manually from the walls of pits dug out by the field operation team. These samples were manually filled into cups on the robotic carousel. Table 1 lists soil samples analyzed and reported in this paper: their locales, depths and collection methods. The locales where samples were collected were given in Fig. 2 on the rover's traverse. The sampling sites were remotely selected by the science team to represent different geological features. Locale 2B was in a flat alluvial fan; locale 5 was about 600 m to the west of locale 6B. Both locale 5 and 6B were next to white colored volcanic ash hills. Locales 8 to 11 were at the north side of the playa. The playa was covered with sediment clays.

Scientific instruments

Zoë rover has a navigation camera on its front mast (Fig. 1), which took panorama images during travel and at the sites along its traverse. In addition, a standoff Vis-NIR spectrometer was installed on the same mast and took spectra of selected targets at a few meters distance.

The MMRS and BUF were installed in the body of the Zoë rover, above the carousel, to analyze *in situ* the subsurface samples delivered by the carousel. Both *in situ* sensors were developed by a combined team at Washington University in Saint Louis and the Jet Propulsion Laboratory. More details of MMRS, BUF and the carousel are shown in Fig. 1. The MMRS[8,9] has a two-unit configuration. A probe unit contains a YAG-KTP crystal pair to generate a 532-nm laser beam for excitation, the optics for laser beam focusing and for Raman photon collection and a step-motoring mechanism that enable a ~1-cm line scan of optical bench of probe unit at sample surface. The main unit of MMRS contains an 808-nm diode pump laser, MMRS Raman spectrometer and detector, electronics for laser driving and control, a microprocessor for commending MMRS operation and data receiving, plus MMRS calibration lamp. MMRS probe unit was installed above the carousel, for *in situ* sensing of the delivered sample in a cup. Two optical fiber cables

Journal of RAMAN SPECTROSCOPY

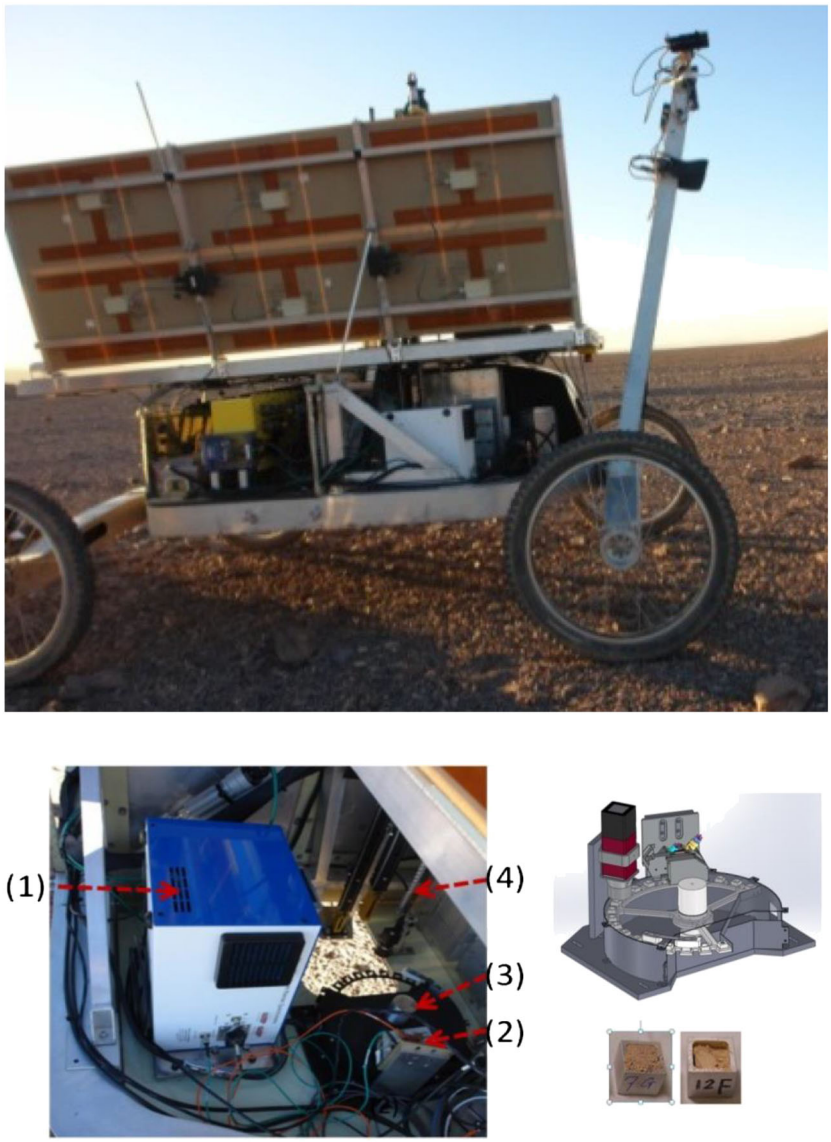

Figure 1. Upper: the Zöe rover with its full payload in the Atacama desert: a Panorama camera and a Vis-NIR spectrometer on the mast, a 1-m drill (view blocked by the solar panel), a carousel, the MMRS and BUF for *in situ* measurements of delivered samples. Bottom left: the MMRS on the Zöe rover: (1) MMRS main unit, (2) MMRS probe unit, (3) the carousal and (4) the drill bit. Bottom right: diagram of the carousal, the MMRS probe unit and the BUF imager; and photos of two 1-cm^3 sample cups (notice different cup fullness).

connect the two MMRS units, one for sending 808-nm laser beam to YAG-KTP pair in probe, and one for sending collected Raman photons to MMRS spectrometer. MMRS spectrometer covers a spectral range from 100 to 4000 cm^{-1}, with a spectral resolution of 7–8 cm^{-1}. MMRS probe has a working distance of ~10 mm from the sample surface and generates a laser beam of 20–30 mW with a diameter <20 μm at the focus. The wavelength calibration of MMRS spectrometer was performed twice using the Ne calibration lamp during the field campaign, and the laser wavelength calibration was performed daily using naphthalene powder filled in a sample cup on the carousel during the field operation.

BUF consists of a set of white and UV (370 nm) LEDs for illumination of the sample, a short-pass filter for wavelength selection of fluorescence emission from the sample and a camera to record the image.[16] It produces two types of images: the contact image of a sample in a cup delivered by carousel and the UV-stimulated fluorescence image of the same sample. An important technical feature of BUF is that it uses a new technology called 'light-field' which allows the image to be taken from the sample of non-even surface without needing of an auto-focusing mechanism. From each sample, BUF generates two image cubes (illuminated by white LEDS and UV LEDS, respectively), from which two all-in-focus images were generated. BUF was installed above the carousel next to the MMRS probe unit, to obtain the images of the same sample surface examined by MMRS.

Field-MMRS and laboratory Raman analyses

At each field site, after all samples were collected into sample cups and put on the carousal, Raman and BUF measurements were carried out. Then, the samples were removed from the cups and put into separate zip-sealed plastic bags. The cups and the drill head were thoroughly cleaned with ethanol and dried for use at next site. After the 2013 field campaign, all samples were brought back to Washington University in St. Louis, and their Raman spectra were acquired with a laboratory Raman spectrometer (Kaiser Hololab

Figure 2. The 50-km traverse made by Zoë Rover in June 2013 in the Atacama Desert, and the sampling locales.

Table 1. Atacama soil samples analyzed by both the MMRS in the field and by the HoloLab 5000 in the lab

Locales		Sample depth (cm)	
	Coordinates	Drill[a]	Manual
2B	−24.7764, −69.6482		0
5	−24.7865, −69.6127		0, ash[b]
6B	−24.7877, −69.6063		80,30,10,0
8	−24.6350, −69.4537	80,30	80,30
9	−24.6349, −69.4540	80,30	80,30,10
10	−24.6342, −69.4541	80,30,10	80,30,10,0
11	−24.6343, −69.4520	80,30,10	80,30,10,0

[a]Drilled samples were captured over a length of 3 cm on the deep flutes of the drill. The depths given are at the lowest end of the length.

[b]Two samples were collected on the surface at locale 6B, one of which is ash-like.

5000—532 nm) to compare with MMRS measurements in the field. The HoloLab 5000 Raman system has similar configuration with the MMRS and comparable performances in optical throughput. It covers 100–4000 cm^{-1} spectral range, with a spectral resolution of 4–5 cm^{-1}. It delivers ~10-mW laser power to the sample with a smaller beam size (6 μm) than MMRS. In Atacama field, a MMRS measurement set generally took a 20-point to 100-point linear scan on each sample, with 50- to 200-ms exposure time and 5 to 20 co-add. The measurement set of each sample using HoloLab 5000 generally took a 50-point line scan, with 2-s exposure time and 10 co-add.

There are three major differences between the field-MMRS and the laboratory Raman measurements: (1) The environmental conditions for field measurements were harsh. On the one hand, the MMRS took measurements both when the rover was travelling on rugged terrains and when the rover was at rest, during the day and at night time, with winds and dusts that are typical in the desert, accompanied by a broad diurnal temperature and relative humility changes. On the other hand, the lab Raman measurements were carried out on a stable anti-vibration table, in a dark, wind and dust free, air-conditioned laboratory room. (2) Only limited time and electric power were available from Zoë in the field. These resources had to be shared among rover driving, drilling, mast instruments measurements and *in situ* instruments (MMRS and BUF) measurements, and many other activities. The resource limitations constrained the longest MMRS acquisition time per spectrum in field to 4 s (200-ms exposure time with 20 co-add), whereas 20 s per spectrum is the ordinary measurement duration (2-s exposure time with 10 co-add) in the lab, or 5 times of the longest MMRS acquisition time in field. As the noise from the cooled CCD detector is dominated by shot noise, the signal to noise of a spectrum, *S/N*, is proportional to the square root of the signal acquisition time, T[17]:

$$\frac{S}{N} \propto \sqrt{T} \tag{1}$$

So, with 5 times longer acquisition time, spectra measured in laboratory are expected to have a signal to noise ratio of 2.2 times higher than the field-MMRS spectra. (3) On Zoë, the MMRS probe unit was installed and aligned in a way that assumed its laser beam focusing plane to be leveled with the top edge of sample cups on the carousel (Fig. 1). MMRS optical design can ensure 1/5 S/N at 0.5-mm off-focus for a quartz sample.[8] However, the actual focusing condition in the field varied largely among samples, depending on the status of the cup filling. In some cases, the sample surface was ~3 mm below the top edge of the sample

Journal of RAMAN SPECTROSCOPY

cup. In the lab Raman measurement, sample surfaces were flattened, and focusing was optimized at the first sampling point in a line-scan using the context microscope image.

MMRS results and discussion

MMRS robustness and its wavelength calibration and accuracy

MMRS robustness

The quality of MMRS spectra is dictated by sample composition, operation situation (exposure time, co-add and focusing) and the instrument's performance which is determined by instrument's optical alignment, laser stability and electronics stability, and is shown as signal sensitivity, noise level and Raman spectra reproducibility. In order to have a good evaluation of the instrument performance, reference Raman spectra were taken several times per day, particularly immediately before or after soil sample measurements, for laser wavelength calibration and MMRS performance checking. Naphthalene, which was recommended as one of Raman standards with many Raman peaks over a large frequency range,[17] was used as the Raman reference during this field trip. Powder of naphthalene was filled into a designated cup on the carousal to avoid contamination. Because naphthalene has high evaporation rate, the sample was added into the cup once daily to keep the cup full. Another recommended Raman reference chemical, acetaminophen,[17] will be used instead of naphthalene for future field operations. For planetary mission, diamond film and olivine crystal are desired calibration target because of their physical stability in harsh environment.

Mechanical and optical instability of the instrument, and/or induced opto-electronic performance variation during the rover transverse, if it was to happen, would show up in the changes of the reference spectra. In Fig. 3 are shown two example reference spectra of naphthalene acquired at the beginning (Day-1, in day time) of Zoë's 50-km traverse, and at the end (Day-10, in evening time). They both show very comparable absolute Raman peak intensities in counts (opto-electronics stability), and relative peak intensities over the whole spectrum (overall optical alignment stability).

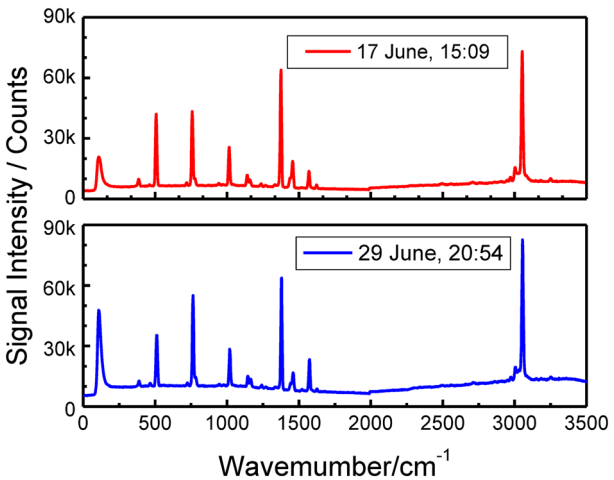

Figure 3. Raman spectra of the reference, naphthalene, acquired at the beginning (upper panel) and the end (bottom panel) of the 2013 LITA field campaign.

Raman peak position accuracy

During the 10-days' field operation, reference Raman measurement was taken 29 times. The standard Raman shifts of the six naphthalene peaks[17] at 3057, 1381, 1022, 766, 513 and 392 cm^{-1} were used to evaluate peak position drifts. We consider two types of drifts generated by different sources. One would be generated by the changes with grating related optics (e.g. thermal) in the MMRS spectrometer, which should produce nonlinear peak drifts, and such nonlinear drifts can be characterized by the change of the standard deviation (σ) of the shifts of the Raman peaks:

$$\sigma = \sqrt{\frac{1}{6}\sum_{i=1}^{6}\left(\left(\nu_i - \nu_i^{std}\right) - \overline{\left(\nu_i - \nu_i^{std}\right)} \right)^2} \qquad (2)$$

where ν_i is the position of one of the 6 peaks, and ν_i^{std} is its standard Raman shift.

The analysis of all the reference spectra shows that all deviations (σ's) are within 1.2 cm^{-1}, which indicates that the grating related optical alignment changes during field campaign can be neglected. Despite rover's 50-km rough transverse path and wide environmental temperature change, from −5.1 °C to 31.1 °C, the MMRS demonstrated robust optical alignment and performance by the conservation of the relative peak positions and the absolute peak intensity counts.

Another type of Raman peak drift, showing as linear offset of the whole spectrum, is mainly related to the laser wavelength change. The offsets of all 29 naphthalene Raman measurement during the field operation are within 6.0 cm^{-1}, with a standard deviation of 3.4 cm^{-1}. This offset is mainly due to the 532-nm laser line shift generated in the MMRS probe unit, which was not temperature controlled and more subject to environmental temperature fluctuation. A new temperature controlling unit will be added to the MMRS probe unit for next field campaign in 2015.

Due to challenging environmental conditions, special attention was paid to obtain accurate Raman peak positions. Each set of Raman measurements on a soil sample was accompanied by a naphthalene Raman measurement taken within half an hour. Comparing to these reference spectra gives about 3-cm^{-1} Raman peak position calibration accuracy. Ideally, each set of Raman measurements on a soil sample should have naphthalene spectra taken immediately before and after spectrum acquisition; however, due to the limited time and power resources during the field campaign, this requirement was not fulfilled.

Furthermore, as each set of multi-point MMRS scan was taken within a short time (10 min), laser wavelength variation due to temperature drift can be neglected. Therefore, a self-calibration methodology can be used to reach the high Raman peak position accuracy determined by the nonlinear drift only. In this methodology, if a Raman spectrum with a well defined peak, such as gypsum peak at 1008 cm^{-1} or quartz peak at 464 cm^{-1}, is present in a set of multi-point line-scan spectra, this peak is used to calibrate the whole set of Raman spectra. Meanwhile, small peak position differences appeared in the same multi-point scan, such as feldspar and TiO_2 polymorphs, as shown in the following sections, can be assigned with high confidence.

Minerals identified from Raman spectra

Multi-point Raman spectra in multiple sets of line scans were acquired for the 30 drill and pit samples, as given in Table 1. The spectral analysis showed the presence of three groups of minerals

in the Atacama soil samples: original igneous minerals (mainly feldspars and quartz), hydrous or anhydrous salts (sulfates and carbonates) with variable origins and carbonaceous materials.

Igneous minerals

Quartz, feldspar and TiO_2 were broadly distributed along the rover traverse, in accordance with previous LITA investigations using X-ray diffraction, thermal infrared emission, visible/near infrared and mid-infrared diffuse reflectance techniques.[5,18]

Quartz

Figure 4 shows typical MMRS spectra of quartz, two TiO_2 polymorphs and two feldspars. Figure 4(a) is a Raman spectrum of quartz acquired by the MMRS for the pit soil sample at locale 9 at the depth of 10 cm. The main peak of quartz is at 464 cm^{-1}; a medium intensity peak is at 204 cm^{-1}; two weak peaks at 128 cm^{-1} and 354 cm^{-1} can also be seen. Quartz is among the most detected minerals in the Atacama soils. Its main peak at 464 cm^{-1} is one the peaks used for spectral self-calibration.

Two TiO_2 polymorphs

Three TiO_2 polymophs, brookite, anatase and rutile can be distinguished by their Raman spectra.[19] In particular, brookite and anatase have strong Raman peak at very low wavenumbers (144 cm^{-1} and 151 cm^{-1}, respectively), which were identified in the Atacama soils. Figure 4(b) shows their typical Raman spectra. The spectra were acquired by MMRS for the drilled soil sample at Locale 9 at 5-cm depth. Another polymorph of TiO_2, rutile, was not observed in the Atacama. The two polymorphs were identified in the same set multi-point line-scan Raman spectra. As discussed above, the position difference of the strongest peaks in the two spectra is clear without the need of detailed Raman shift calibration. Furthermore, the three peaks in the Raman spectrum of anatase at 392, 512 and 632 cm^{-1} taken by MMRS are consistent with the peak positions of anatase spectrum in RRUFF spectral database (http://www.rruff.info).

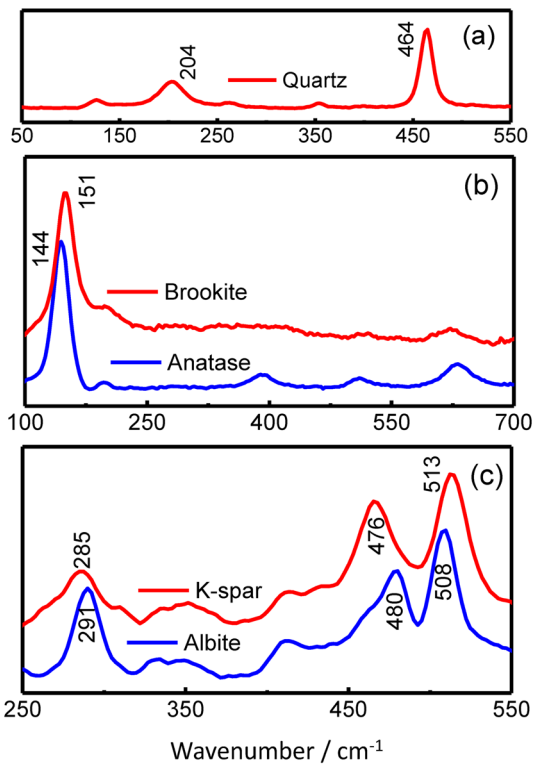

Figure 4. Typical Raman spectra of (a) quartz, (b) two types of TiO_2 and (c) two type of feldspars acquired by the MMRS in the 2013 LITA field campaign.

Two types of feldspars

Feldspars consist of three end-member groups: anorthite (Ca-feldspar), albite (Na-feldspar) and K-feldspar. The detailed crystallization and Raman peak positions and widths also depend on formation temperature. The Raman spectra of a large number of feldspars were obtained in a detailed investigation aimed for planetary exploration, which shows the spectral features (spectral pattern, peak positions and widths) that can be used to distinguish among the end-members and compositional/structural intermediate solid-solutions.[20] Two typical Raman spectra, acquired by MMRS for the pit sample at locale 9 at 80-cm depth, are shown in Fig. 4(c). These spectra can be best assigned to low albite and maximum microcline. These two MMRS spectra were acquired in one set of multi-point line scan. The position difference of the major Raman peaks of these two types of feldspar is obvious; thus, the identification bears high precision without the need of detailed Raman shift calibration. In consistence with the standard spectra,[20] the main peak of albite has a slightly smaller Raman shift (508 cm^{-1}) than maximum microline (513 cm^{-1}), while the second peak of albite has a slightly bigger Raman shift. The positions of the third peak at about 290 cm^{-1} are also consistent with the assignment. Although ten types of feldspars were identified solely on the basis of their Raman spectra,[20] such classification requires the Raman shift accuracy to be less than 1 cm^{-1} and often needs observation of relatively weak peaks. The three end-member feldspars, K-feldspar, albite (Na-feldspar) and anorthite (Ca-feldspar), have the strongest Raman peaks at 513, 508 and 505 cm^{-1}, respectively. The strongest Raman peaks observed *in situ* and in lab for the Atacama feldspars are between 508 and 516 cm^{-1}, indicating that alkali-feldspars are dominant. In some cases, particularly, for the pit sample at locale 9 at 30-cm depth, spectra can be best assigned to ternary feldspars,[20] with most contributions from alkali-feldspars.

Two types of carbonates

Almost all carbonates identified in the Atacama soils by MMRS and laboratory Raman measurements are calcite. No dolomite was identified. They were found mainly in locale 6B, and minor amounts were found in locale 10 in the playa.

Raman spectra of carbonates have the characteristic bands due to the internal modes of the anion group, of which the strongest is the symmetric stretch $\nu_1(CO_3)$.[21,22] A typical calcite Raman spectrum, acquired by MMRS of the pit sample at locale 6B at 10-cm depth, is shown in Fig. 5. The bands at 713 cm^{-1} and 282 cm^{-1} are due to the internal $\nu_4(CO_3)$ symmetric bending, and an external mode involving translation of the anion groups, respectively.[21,22] The standard calcite Raman spectrum is also given in Fig. 5, in the bottom panel. A second type of carbonate, with the $\nu_1(CO_3)$ band shifted to 1066 cm^{-1}, also shown in Fig. 5, was observed as a minor phase for the pit sample at locale 6B at 80-cm depth. No such spectra were observed in the other samples. The frequency is close to ν_1 in free CO_3^{2-} group and might be due to K_2CO_3, or $BaCO_3$.[21] Potassium is present in the region in feldspars. Besides the carbonates, the two MMRS carbonate spectra also have bands of two other phases, gypsum at 1008 cm^{-1} and quartz at 464 cm^{-1}.

Journal of RAMAN SPECTROSCOPY

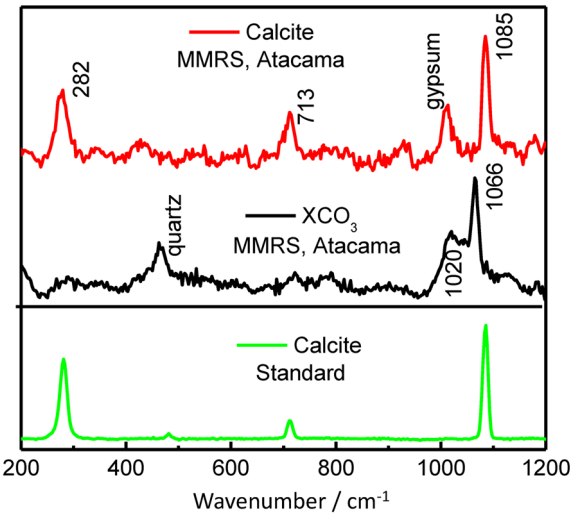

Figure 5. Typical MMRS spectra of carbonates (upper panel), compared with standard calcite Raman spectrum (bottom panel).

Three types of sulfates

Raman spectra of sulfates. Three calcium sulfates, gypsum ($CaSO_4{\cdot}2H_2O$), natural anhydrate (β-anhydrite) and γ-anhydrite were identified in Atacama soils both by field-MMRS and by laboratory Raman analysis. For simplicity and in accordance with most literature reports, the natural anhydrate (β-anhydrite) is referred to as anhydrite in this paper. Another stable calcium sulfates, bassanite ($CaSO_4{\cdot}0.5H_2O$), was not observed. Gypsum and anhydrite are among the most abundant minerals identified in the Atacama soils, while the third Ca-sulfate, γ-anhydrite, was observed as a minor phase.

In Fig. 6, upper panel, the gypsum and anhydrite Raman spectra were acquired by MMRS for the surface ash sample at locale 5 and the pit sample at locale 6 at 80-cm depth, respectively. Raman spectrum of γ-anhydrite was observed by MMRS for the drill sample at locale 9 at the depth of 30 cm. In order to present the full spectral details for a firm identification of γ-anhydrite, a Raman spectrum of this mineral taken from the same soil sample using HoloLab 5000 Raman spectrometer with higher signal-to-noise ratio is given in Fig. 6. Raman spectra of calcium sulfates bear many similarities as the peaks are due to internal vibrations of the sulfate anion group, in the spectral region from 400 to 1200 cm^{-1}, and from OH stretching vibration in the water moiety, from 3400 to 3620 cm^{-1}. The exact peak positions are affected by structural changes (bond length and angles) of SO_4 tetrahedra and hydration degree.[23–25] The symmetric SO_4 stretching vibration (ν_1) produces the strongest Raman peak near 1000 cm^{-1}. The ν_2 (SO_4) symmetric bending frequencies and ν_4 (SO_4) asymmetric bending frequencies are from 415 cm^{-1} to 500 cm^{-1} and from 610 cm^{-1} to 676 cm^{-1}, respectively.

Raman spectra of gypsum are easily distinguished from other Ca-sulfates based on the double water peaks and the main peak at 1008 cm^{-1}. The main peak positions of anhydrite (1017 cm^{-1}) and bassanite (1015 cm^{-1}) are too close to be clearly distinguished from each other in field-MMRS spectra with the Raman peak position uncertainty of about 3 cm^{-1}. However, when considering other peaks, the differences in the Raman spectra of anhydrite and bassanite are clear. In particular, OH stretching peaks are present in bassanite but not in anhydrite. In the region from 600 to 680 cm^{-1}, anhydrite has three peaks, while bassanite only has

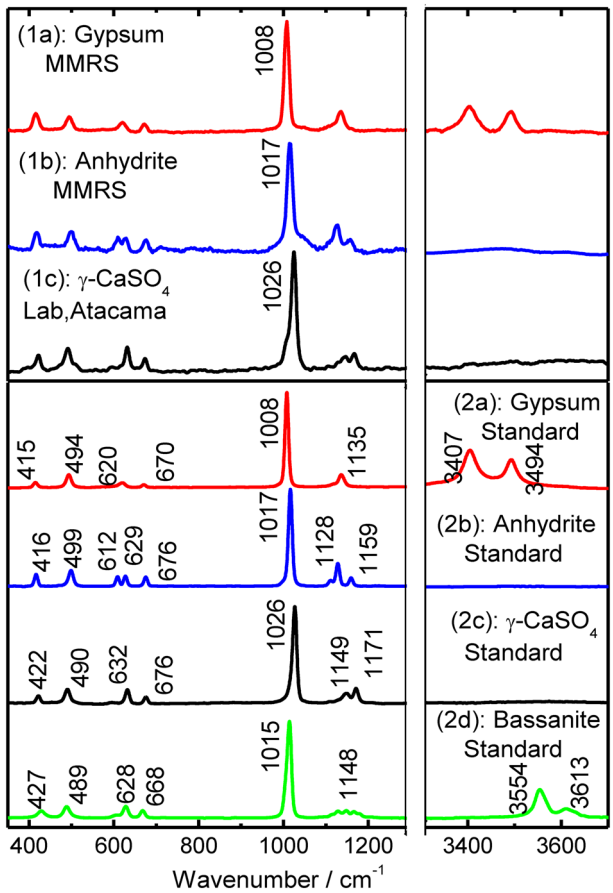

Figure 6. Typical Raman spectra of three identified calcium sulfates in the Atacama soils (upper panel), and Raman spectra of four standard Ca-sulfates (bottom panel).

two. In both field-MMRS and laboratory-acquired spectra, no OH stretching peak, one of the most clear distinguishing features, was observed that can be assigned to bassanite. All other weak peaks also support the presentation of anhydrite but not bassanite. Therefore, though there are some low S/N Raman spectra in which only the main peak of sulfates near 1015–1017 cm^{-1} is clear, we conclude that they are due to anhydrite but not bassanite.

Raman spectrum of γ-anhydrite were reported as the product from low-temperature (T < 110 °C) dehydration of gypsum.[26–28] Compared to Raman spectra of other calcium sulfates, the main peak of γ-anhydrite has a relatively large Raman shift, at 1026 cm^{-1}, and as anhydrite, it has no water peaks. γ-Anhydrite was observed by MMRS in the pit sample at locale 8 at 80-cm depth. It was observed more frequently in the lab as a minor phase in the Atacama samples. Especially, larger amount of γ-anhydrite (20%, derived from point counting analysis as described in section 'Point counting methodology'), was observed in the drill sample at locale 10 at 30-cm depth.

Laboratory dehydration of gypsum and stability of γ-anhydrite. Commercial gypsum (Alpha Aesa, 98.0–102.0%, CAS # 10101-41-4), anhydrite (Sigma-Aldrich, 237132-100G-325 mesh, 99%, CAS # 7778-18-9) and bassanite chemicals (Sigma-Aldrich, 98%, 307661-25G, CAS # 10034-76-1) were used to take standard Raman spectra, shown in Fig. 6(2a), (2b) and (2d). The standard sample of γ-anhydrite, Fig. 6(2c), was produced by dehydration of gypsum in an oven at 105 °C. It was found that γ-anhydrite

(main Raman peak at 1026 cm^{-1}) re-hydrated very quickly into bassanite (main Raman peak at 1015 cm^{-1}) within minutes, under laboratory room environment (20 °C, 10% RH). No gypsum dehydration process was observed at T < 55 °C over one week, while bassanite was observed from dehydration of gypsum after 3 days in an oven at 65 °C.

Carbonaceous materials. Raman spectra from carbonaceous materials were observed by the field-MMRS and the laboratory Raman measurements, as a minor phase, and were only observed in the samples in the playa (locales 8–11) without depths preference. Figure 7 shows a MMRS spectrum of the Atacama soil at locale 8 at 80-cm depth and two laboratory measured spectra of the Atacama soil at locale 9 at 80-cm depth. Pure graphite shows a peak at 1582 cm^{-1} (G-band). With increased disorder in structure, two broad Raman peaks (the D-band and G-band) and a peak shoulder (D′) at 1355, 1581 and 1620 cm^{-1} were observed.[29] Exact bands' shapes and positions are determined by the detailed structure, and the peak area ratio of D- and G-band is used to quantify the structural order of these C-bearing phases, which is related to their formation temperatures or later metamorphic processes.[30] The Raman spectra of carbonaceous materials obtained by MMRS in field and by HoloLab5000 in laboratory show highly variable relative intensities of D- and G-bands (Fig. 7) in the Atacama samples, which suggest a large range of conditions in their formation. The BUF images taken from these playa samples are under analysis.

Mineral phase distributions in the region explored by the rover

Point counting methodology

After the minerals were identified based on their characteristic Raman spectra, the next step was to find how much each of them was present in each soil samples and their overall distributions in the region explored by Zoë. It has been long recognized that to determine the mineral proportions in a mixture (rock or soil) based on Raman peak intensities in a LRS spectrum is impractical,[31] because too many uncontrollable and uncorrectable factors affect the absolute Raman peak intensities. Such factors include un-known Raman cross sections of mineral phases, crystal orientation of a mineral grain in the sample, laser focus condition during a line scan and laser emission fluctuation following the change of environmental conditions. Instead, we used a point counting methodology,[31] in analogy with the standard petrographic technique of point counting, to determine mineral proportions in a sample through multi-point line scanning. As MMRS uses a narrow laser beam, only one or a few mineral grains were excited in one spot (<20 μm), which generated the spectra shown in Figs. 4–7 with a single, or two to three phases. From a multi-point line scan, 50–100 Raman spectra were acquired, and the proportion of each mineral, in percentage, was estimated from the fraction of the spectra in which the characteristic peaks of that mineral appear.

$$Proportion = \frac{\sum_i 1/f_i}{N} \cdot 100\% \quad (3)$$

where, N is the number of points, i.e. number of Raman spectra, in the multi-point line scan; the summation was made over all spectra in which characteristic peaks of the mineral were present and f_i is the number of phases in the i^{th} spectrum. We found that f_i is from 1 to 3 in both the field-MMRS and laboratory-HoloLab spectra.

Comparison of four approaches

Based on the three reasons listed in section 'Field-MMRS and laboratory Raman analyses', the Raman spectra obtained in laboratory are expected to have better S/N ratios than those from field-MMRS measurements, even though with similar instruments. Furthermore, in the field, the sample cups filled manually by the field operation team had less focusing issue than the sample cups filled autonomously by the drill. In order to understand the effects of the above factors on the final result, and to gain an overall understanding of the regional mineralogy distribution, we needed to compare the results from the four sets of measurement approaches: (1) MMRS measurements, drill-extracted samples and drill-filled sample cups (MMRS-Drill); (2) MMRS measurements, manually collected pit samples and manually filled sample cups (MMRS-Pit); (3) Lab-Raman measurements, drill-extracted samples (Lab-Drill); and (4) Lab-Raman measurements, manually collected pit samples (Lab-Pit). Raman focusing was manually optimized before each Raman line-scan in approaches (3) and (4) based on checking of context image focusing; however, in approaches (1) and (2), how well the MMRS was focused depended on whether the sample was filled to the designed focal plane—the top edge of the sample cups.

As shown in Table 1, each of the 10 drilled samples has a corresponding manually collected pit sample to evaluate the automated drill sampling and sample delivery processes. Raman spectra of the same set of soil samples were acquired using the laboratory Raman spectrometer to compare with MMRS' field measurements. Therefore, the samples at locales 8 to 11 in the playa provide good comparison cases. Figure 8 shows minerals identified and their proportions at locale 10 (from 3 depths, 10 cm, 30 cm and 80 cm) by the four approaches. In addition, we used 'informative spectra' to name the spectra that contained at least one useful Raman peak for phase identification. Table 2 presents the ranges of percentages of 'informative spectra' among all spectra obtained from multi-point linear scan. The ranges of percentages were compiled from the data obtained from the 10 drill samples and the corresponding pit samples (excluding manually collected surface samples, see Table 1) at locales 8–11 in the playa.

The most important conclusion revealed by Fig. 8 is that all four approaches give similar big pictures on mineral distributions, i.e. a high proportion of anhydrite found at the greatest depths (80 cm) and a high concentration of gypsum found at shallow depth (10 cm), with less variable proportions of other mineral phases at different depths.

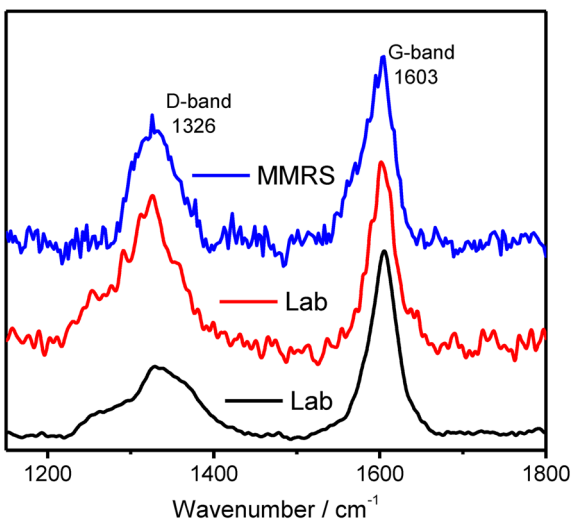

Figure 7. MMRS and laboratory measured Raman spectra of carbon in the Atacama soils.

Journal of RAMAN SPECTROSCOPY

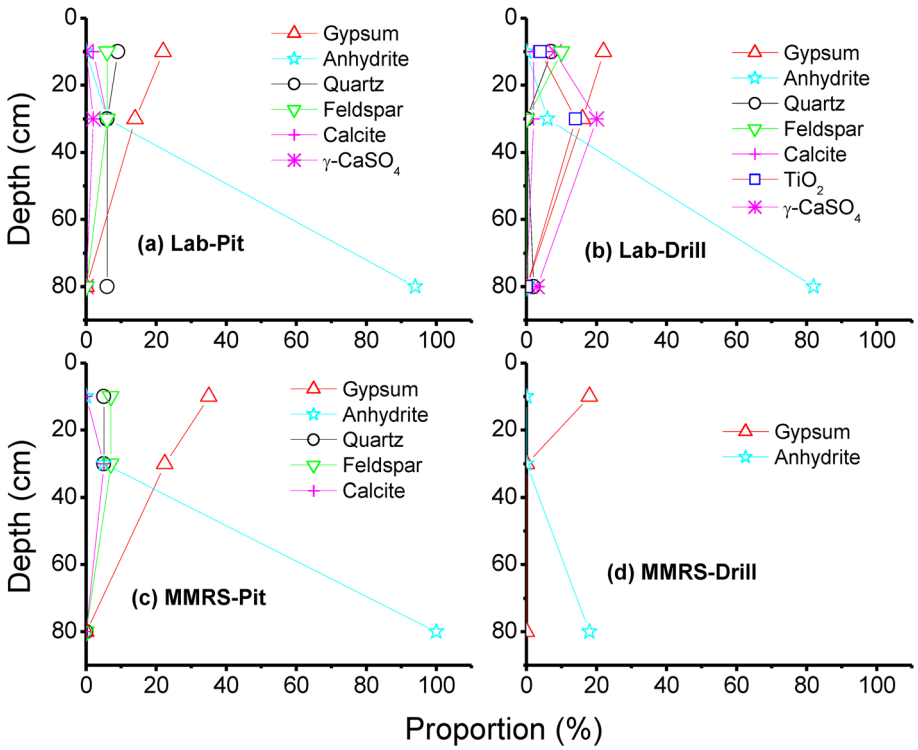

Figure 8. Comparison of minerals identified and their proportions obtained from 4 approaches at locale 10.

Table 2. Percentages of informative Raman spectra by different approaches

Approach	Informative percentage range[a]
Lab-Pit	36%–100%
Lab-Drill	10%–87%
MMRS-Pit	10%–100%
MMRS-Drill	0%–30%

[a]The range is for the 10 drilled samples and the corresponding pit samples in Table 1.

Furthermore, we can make three additional comparisons to elucidate performances of these different approaches. (1) Comparison of laboratory measurements of pit samples (Fig. 8(a), Lab-Pit) and drill samples (Fig. 8(b), Lab-Drill) shows very similar results, indicating that samples of comparable mineral compositions were collected by the two sampling approaches. However, when considering the percentages of informative spectra obtained from these measurements on samples from all four locales in the playa, i.e. Table 2, the percentage range of informative spectra of drilled samples (10–87%) is slightly less than that of pit samples (36–100%). Because when soils were brought up by the drill from depth, large grains tended to fall off from the drill flutes, especially for non-cohesive soils; thus, the extracted soil samples tended to have smaller grain sizes than manually collected pit samples. As light scattering (laser photons and Raman photons) occurs at grain boundaries, a sample with fine grain sizes generally has less strong Raman signals. (2) Comparison can be also made between laboratory Raman and field-MMRS measurements of the pit samples (Fig. 8(a), Lab-Pit; and (c), MMRS-Pit). As pit samples were manually filled to the top of sample cups, MMRS' focusing conditions were well satisfied. The comparison shows very close results from the two sets of measurements, though the field MMRS measurement reveals higher proportion of gypsum and laboratory Raman measurement (with a smaller beam diameter) shows slightly higher proportions of minor phases, particularly γ-anhydrite. Comparing the percentage ranges of informative spectra of laboratory Raman and field-MMRS measured pit samples (Lab-Pit and MMRS-Pit in Table 2) MMRS has a comparable but slightly lower informative percentage. Given the effect of harsh field environment conditions on hardware and the short acquisition time for field MMRS measurements, these results demonstrate that MMRS has a comparable performance as the laboratory instrument when its focusing condition was satisfied. (3) Spectra of MMRS-measured drill-filled samples are less informative among the four, in a percentage range from 0 to 30% (Table 2), shown in Fig. 8(d) as well. This significantly poor performance is obviously the result of poor filling (autonomously by the drill) of sample cups in some cases, which caused out-of-focus performance of the MMRS. In other cases, the fully autonomous process worked and provided highly informative MMRS spectra for mineral identification. For example, the typical TiO_2 spectra in Fig. 4 were obtained by the all automated MMRS-Drill approach. As mentioned in section 'Sampling and sample delivering', the drill has now been modified to collect samples more effectively in porous soils. To autonomously acquire representative subsurface samples and to deliver them in a way that satisfy the focusing condition of *in situ* sensors (e.g. MMRS) is a lesson learned by the 2013 field campaign, and steps have been taken to correct this issue for the 2015 field campaign.

Mineral distributions on the surfaces and over the depths

Since different measurement approaches gave similar big pictures about mineral distributions, for simplicity and clarity, we will not

present the results of each approach, but averaged them. Because of the out-of-focus issue with the MMRS measurements of drilled samples, they are excluded in the averaging. The results are shown in Fig. 9. Also for clarity, only minerals with a proportion bigger than 5% are plotted in the figure.

Surface distributions. Mineral distributions at the surfaces outside of the playa (Fig. 9(a)) show that the region is covered mainly by feldspars and quartz. However, at locale 5, an ash sample collected on the surface is composed almost purely of gypsum. At locale 6B (Fig. 9(b)), just below the surface at 10-cm depth, calcite was found to be the most abundant mineral. At locale 10 in the playa (Fig. 9(e)), the most identified mineral at surface is also gypsum. TiO_2 was identified at the surface with comparable amount as quartz at locale 11 in the playa (Fig. 9(f)). Such surface mineral distributions may be compared with orbital remote sensing and field standoff sensing using Vis-NIR spectroscopy that yield surface composition and mineralogy distributions.

Depth distributions. While feldspars and quartz occur broadly in the region, they seem to have higher abundance near the surface, with the only exception at local 11. Gypsum appears in the region, without obvious depth preference (except at locale 10). Anhydrite shows higher abundance in deeper depth at both locale 6B and 10, where it is present. Anhydrite should be a direct product from high temperature processes, e.g. volcanic, because the dehydration of gypsum would form first bassanite that is very stable below 100 °C.[32] Gypsum occurs more broadly inside the playa, in three out of four locales, than outside. The gypsum might originate as a product of sedimentary process, e.g. precipitation from Ca-SO_4-rich brines. γ-Anhydrite was identified as a minor phase, with an exception at locale 10 in the playa. Similar to anhydrite, γ-anhydrite might be a product from igneous processes, it could also be a dehydration product from sedimentary gypsum at high temperature (>110 °C). However, finding stable γ-anhydrite, with a quite large quantity (20% in a sample at locale 10 at 30-cm depth) in the Atacama soils, raises an important question on its stability field. This observation is consistent with the discovery of γ-anhydrite as one of the vein filling sulfates in martian meteorite MIL03346.[33,34] Both these findings are contradictory with a past laboratory investigation on dehydration of gypsum[32] using fine-controlled temperature and humidity, showing bassanite forms rapidly from γ-anhydrite under low relative humidity (<1%RH) and low temperature (258 K). Our experiments (section 'Laboratory dehydration of gypsum and stability of γ-anhydrite') also demonstrated completion of the same phase transformation within a few minutes at 20 °C, 10% RH. The discrepancy between above laboratory results and field observation suggests a potential mechanism in natural settings that may have prevented the fast rehydration of γ-anhydrite. Coexisting mineral assemblage was found to have catalytic effect that can modify the meta-stability of a hydrous Mg-sulfate,[35] more experimental investigations are obviously needed to address this discrepancy.

Carbon is a minor phase with proportions < 2%. It is only observed in the soils in the playa. No distribution preference could be identified in terms of depths or sampling methods (drill or manual).

Implications for the exploration of Mars

Mineral identification

Orbiter- and rover-based studies of rocks and regolith on Mars have revealed a diverse mineralogy. Hydrous calcium sulfates, including both gypsum and bassanite, had been inferred from OMEGA and CRISM observations (using Vis-NIR spectroscopy based on orbital remote sensing) in multiple locations on Mars.[36,37] Veins of Ca-sulfate, believed to be gypsum, have been found by the

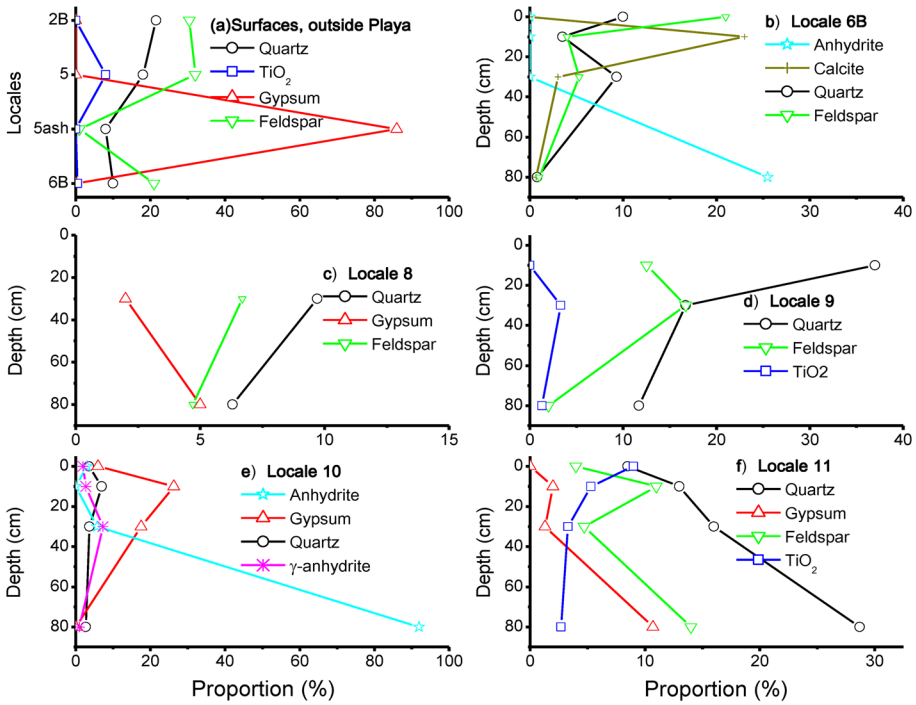

Figure 9. Main minerals (with a proportion > 5%) distributions. a): on surfaces at locales 2B, 5, and 6B. b)–f): over depths at locale 6B, and 8–11 in the playa. See the text for the details.

Opportunity rover at the western edge of Cape York on the rim of Endeavor Crater.[38] Plagioclase feldspar was detected as one of the main phase, with quartz, anhydrite, bassanite as minor phases, in a mudstone at Yellowknife Bay, Gale crater, by Curiosity rover.[39] The existence of carbonate minerals on Mars has long been postulated, based on evidence of past and present water along with a CO_2-rich atmosphere.[40] Carbonate minerals have been observed in a range of Martian geological materials, including dust, bedrock outcrops and several meteorites.[40–44]

As demonstrated by MMRS through the 2013 Atacama field campaign, laser Raman spectroscopy will be a powerful tool for *in situ* definitive mineral characterization and detection of carbonaceous materials during landed missions on Mars. It will provide valuable insight into the evolution of habitats, atmosphere and climate on Mars. However, Raman scattering is an intrinsically weak process. It requires a carefully crafted optical configuration with high optical efficiency in order to collect decent Raman signals from mineral mixtures of complicated natural materials (rocks and regolith with rough grain surfaces) for a robotic planetary surface exploration mission. Through the past 20 years' studies and tests in the laboratory and in natural geological settings, we have developed what we consider the best configuration for a planetary Raman system to satisfy the needs of fine-scale definitive mineralogy and biomarker detection, i.e. a micro-beam Raman unit using the most mature, and optically most effective techniques, e.g. continuous wave, low power 532-nm laser, visible optics and ordinary CCD, which is the configuration of the MMRS and its next version CIRS (Compact Integrated Raman Spectrometer). Supported by NASA MatISSE program, a prototype of CIRS was built in 2014 and is undergoing optimization.[10]

Seek the signs of life

The first few hundreds of millions of years of Mars' geologic history have recorded surface environments that differ considerably from the present surface conditions, prompting a succession of coordinated surface and orbiter missions over the past two decades aimed ultimately at determining if Mars ever had an early biosphere. Past missions have sought environments where water was abundant and possibly long-lived. The Curiosity rover has shown that Gale Crater once possessed a habitable fluvio-lacustrine environment at Yellowknife Bay.[39] Although Curiosity suggested that indigenous martian or meteoritic organic carbon sources may be preserved,[38] the definitive detection of organic matter by SAM (Sample Analysis at Mars) on Curiosity was complicated by the sample preparation process, i.e. sample heating.[45] At heated temperature, perchlorates, which is pervasive on Mars, burnt organic substances into single carbon compounds.[45,46] Contamination effect that could interfere with martian signal detection also needed to be removed from such analysis.[45–48] MMRS-CIRS uses noninvasive technique thus can investigate a sample as it is. Moreover, as MMRS-CIRS measurement is very rapid, with the analysis of each sampling point in a line scan that can be completed in seconds, generating hundreds spectra in each set of measurements during a martian sol, thus increasing the probability of encountering biosignatures.

Field-MMRS and laboratory Raman measurements on the collected samples from the 2013 field campaign traverse have detected carbonaceous materials in many cases, but have not detected organic matters. Previous field investigations in Atacama Desert indicated that drier interior regions are less microbially rich.[2,49] The microbial colonization of Ca-sulfate crusts was found to be related to relative humidity, abundant at one site but scarce at a drier site.[11] Our findings confirmed that microbial life is very rare in soils of the hyper-arid core desert region, since no life-related organic compounds were detected.

In an experimental study on the detection limit of *in situ* green Raman configuration (MMRS-CIRS-like), we have demonstrated a detection sensitivity of carbonaceous materials at 8×10^{-6} w/w in mixtures of an Archean chert with quartz, and the detection sensitivity of four bio-markers, N-acetyl-L-phenyialanine, cholesterol, octadecane and β-carotene at mole concentration from 10^{-3} to 10^{-5} in mixtures with gypsum.[50] It suggests that if bio-makers of that concentration exist in a localized point in a sample, they will be detected.

Conclusion

The 10-day 2013 LITA field campaign in the Atacama Desert demonstrated the ruggedness of the MMRS. The automated soil sample analysis made by the MMRS unambiguously identified a variety of igneous minerals (quartz, feldspars and TiO_2 polymorphs), carbonates, sulfates and carbonaceous materials. The field-MMRS identifications were confirmed by laboratory Raman analysis, which showed that the MMRS has a comparable performance as the laboratory instrument when its focusing condition was satisfied. Quantified distributions of major minerals and carbonaceous materials are extracted from the measurements, which can indicate regional geological evolution, and potential bioactivities.

Through this first time integrated autonoumous drilling-sampling-sensing exercise in a natural environment, we learned the challenging issues associated with the drill, the sample presentation to *in situ* sensors and the sensor calibration. Technical modifications will be made in preparation of the next field campaign.

Acknowledgements

We gratefully acknowledge NASA support through ASTEP fund NNX09AE80A and MATISSE fund NNX13AM22G. We thank the members of LITA Science team (Gredon Foil, Edmond Grin, Trent Hare, Jeffrey Moersch, Kenneth Tanaka, Christopher Tate and David Thompson), the members of LITA engineering team (James Teza, David Kohanbash, Srinivasan Vijayarangan, Gale Paulsen, Bolek Mellerowicz, Sean Yoon, Jack Craf and Magnus Hedlund) and LiTA team's Chilean collaborators Dr. Guillermo Chong and Dr. Cecilia Demergasso. We appreciate very much the generous supports that have been given by the Department of Earth and Planetary Sciences and the McDonnell Center for Space Sciences at Washington University in St. Louis, and by the Division 42 and 38 of Jet Propulsion Laboratory to MMRS-CIRS project.

References

[1] H. Bao, K. A. Jenkins, M. Khachaturyan, G. Chong-Diaz Earth Planet, *Sci. Lett.* **2004**, *224*(3–4), 577.
[2] A. C. Nathalie, D. Wettergreen, K. Warren-Rhodes, et al. G04S02, *J. Geophys. Res.* **2007**, 112.
[3] C. McKay, E. I. Friedman, B. Gómez-Silva *Astrobiology* **2003**, *3*, 393.
[4] K. Warren-Rhodes, J. L. Dungan, J. Piatek et al., *J. Geophys. Res.* **2007**, 112, G04S15.
[5] B. Sutter, J. B. Dalton, S. A. Ewing, et. al., *J. Geophys. Res.* **2007**, *112*, G04S10.
[6] N. A. Cabrol, D. S. Wettergreen. LPI contribution no. 1612 **2011**.
[7] A. Wang, L. Haskin, E. Cortez *Appl. Spectros.* **1998**, *52*, 477.

[8] A. Wang, L. A. Haskin, A. L. Lane, et al. *J. Geophys. Res.* **2003**, *108*(E1), 5005.
[9] A. Wang Alian, 43rd Lunar and Planetary Science Conference; Abs# 2149, March 19–23, **2012**, The Woodlands, Texas, USA.
[10] A. Wang et al., 2nd International Workshop on Instrumentation for Planetary Missions, Abs# 1090, November 4–7, Greenbelt, Maryland, USA, **2014**.
[11] J. Wierzchos, B. Camara, A. Delosrios, et al. *Geobiology* **2011**, *9*, 44.
[12] S. A. Connon, E. D. Lester, H. S. Shafaat, D.C. Obenhuber, A. Ponce. *J. Geophys. Res.* **2007**, *112*, G04S17.
[13] Y. Bar-Cohen, K. Zacny, *Drilling in Extreme Environments Penetration and Sampling on Earth and Other Planets*, John Wiley & Sons, Weinheim, **2009**.
[14] K. Zacny, K. G. Paulsen, S. Yoon, D. Wettergreen, N. Cabrol, 45th Lunar and Planetary Science Conference, Abs#1174, March 17–21, **2014**, The Woodlands, Texas, USA.
[15] K. Zacny, G. Paulsen, C. P. McKay, et al. *Astrobiology* **2013**, *13*, 1166.
[16] A. Wang, J. Lambert, P. Sobron, 44th Lunar and Planetary Science Conference, Abs# 2586, March 18–22, **2013**, The Woodlands, Texas, USA.
[17] R. L. McCreery, *Raman Spectroscopy for Chemical Analysis*, John Wiley & Sons Inc., New York, **2000**.
[18] J. L. Piatek, C. Hardgrove, J. E. Moersch, et. al., *J. Geophys. Res.* **2007**, *112*, G04S04.
[19] H. G. M. Edwards, N. F. Hassan, P. S. Middleton *Anal. Bioanal. Chem.* **2006**, *384*, 1356.
[20] J. Freeman, A. Wang, K. E. Kuebler, B. L. Jolliff, L. A. Haskin *The Canadian Mineralogist* **2008**, *46*, 1477–1500.
[21] N. Buzgar, A. I. Apopei *Geologie. Tomul LV* **2009**, *2*, 97.
[22] P. Gillet, in *Handbook of Vibrational Spectroscopy*, *Vol. 4*, (Eds: J. M. Chaimers, P. R. Griffiths) John Wiley and Sons, Chichester, **2002**, pp. 3169–3191.
[23] E. Susana, J. Villar, H. G. M. Edwards *Anal. BioAnal. Chem.* **2006**, *384*, 100.
[24] L. Yang, A. Wang, J. J. Freeman, 40th Lunar and Planetary Conference, March 23–27, **2009**, The Woodlands, Texas, USA.
[25] B. J. Berenblut, P. Dawson, G. R. Wilkinson *Spectrochim. Acta* **1973**, *29A*, 29.
[26] G. A. Lager, T. Armbruster, F. J. Rotella, J. D. Jorgensen, D. G. Hinks *Am. Mineral.* **1984**, *69*, 910.
[27] P. Prasad, A. Pradhan, T. N. Gowd *Curr. Sci.* **2001**, *80*, 1203.
[28] C. H. Chio, S. K. Sharma, D. W. Muenow *Am. Mineral.* **2004**, *89*, 390.
[29] T. Livneh, T. L. Haslett, M. Moskovits *Phys. Rev. B* **2002**, *66*, 195110.
[30] J. D. Pasteris, B. Wopenka *Astrobiology* **2003**, *3*, 727.
[31] L. Haskin, A. Wang, K. Rockow, B. Jolliff, R. Korotev, K. Viskupic *J. Geophys. Res.* **1997**, *102*, 19293.
[32] K. Robertson, D. Bish *Icarus* **2013**, *223*, 407.
[33] A. Wang, R. L. Korotev, B. L. Jolliff, Z. C. Ling, submitted to *Planet. Space Sci.*.
[34] Z. C. Ling, A. Wang, 11th International GeoRaman Conference, Abs# 5089, June 15–19, **2014**, St. Louis, Missouri, USA.
[35] A. Wang, J. Freeman, B. L. Jolliff. *J. Geophys. Res.* **2009**, *114*, E04010.
[36] Y. Langevin, F. Poulet, J. P. Bibring, B. Gondet *Science* **2005**, *307*, 1584.
[37] J. W. Wray, S. W. Squyres, L. H. Roach, et al. *Icarus* **2010**, *209*, 416.
[38] S. W. Squyres, R. E. Arvidson, J. F. Bell, et al. *Science* **2012**, *336*, 570.
[39] D. T. Vaniman, D. L. Bish, D. W. Ming, et al. *Science* **2013**, *343*, 1243480.
[40] J. L. Bandfield, T. D. Glotch, P. R. Christensen *Science* **2003**, *301*, 1084.
[41] W. V. Boynton, D. W. Ming, S. P. Kounaves, et al. *Science* **2009**, *325*, 61.
[42] B. L. Ehlmann, J. F. Mustard, S. L. Murchie, et al. *Science* **2008**, *322*, 1828.
[43] J. R. Michalski, P. B. Niles *Nat. Geosci.* **2010**, *3*, 751.
[44] R. V. Morris, S. W. Ruff, R. Gellert, et al. *Science* **2010**, *329*, 421.
[45] R. A. Kerr *Science* **2014**, *343*, 1419.
[46] R. A. Kerr *Science* **2013**, *340*, 138.
[47] J. L. Bada *Science* **2012**, *337*, 1604.
[48] C. Freissinet, D. P. Glavin, S. Kashyap, et al., 45th Lunar and Planetary Science Conference, Abstract # 2796, Mar. 17–21, 2014, The Woodlands, Texas, USA.
[49] K. Warren-Rhods, S. Weintein, J. Dohm et al., *J. Geophys. Res.* **2007**, *112*, G04S05.
[50] J. Wei, A. Wang. Y. Liu et al., 45th Lunar and Planetary Science Conference, Abstract # 2847, Mar. 17–21, **2014**, The Woodlands, Texas, USA.